JOC The Journal of Organic Chemistry

pubs.acs.org/joc Article

Synthesis, Characterization, and Application of a Highly Hydrophilic Triarylmethyl Radical for Biomedical EPR

Urikhan Sanzhaeva, Martin Poncelet, Oxana Tseytlin, Mark Tseytlin, Marieta Gencheva, Timothy D. Eubank, Valery V. Khramtsov, and Benoit Driesschaert*

Cite This: J. Org. Chem. 2020, 85, 10388–10398 Read Online

ACCESS | Metrics & More | Article Recommendations | Supporting Information

ABSTRACT: Stable tetrathiatriarylmethyl radicals have significantly contributed to the recent progress in biomedical electron paramagnetic resonance (EPR) due to their unmatched stability in biological media and long relaxation times. However, the lipophilic core of the most commonly used structure (Finland trityl) is responsible for its interaction with plasma biomacromolecules, such as albumin, and self-aggregation at high concentrations and/or low pH. While Finland trityl is generally considered inert toward many reactive radical species, we report that sulfite anion radical efficiently substitutes the three carboxyl moieties of Finland trityl with a high rate constant of 3.53×10^8 M^{-1} s^{-1}, leading to a trisulfonated Finland trityl radical. This newly synthesized highly hydrophilic trityl radical shows an ultranarrow linewidth (ΔB_{pp} = 24 mG), a lower affinity for albumin than Finland trityl, and a high aqueous solubility even at acidic pH. Therefore, this new tetrathiatriarylmethyl radical can be considered as a superior spin probe in comparison to the widely used Finland trityl. One of its potential applications was demonstrated by *in vivo* mapping oxygen in a mouse model of breast cancer. Moreover, we showed that one of the three sulfo groups can be easily substituted with S-, N-, and P-nucleophiles, opening access to various monofunctionalized sulfonated trityl radicals.

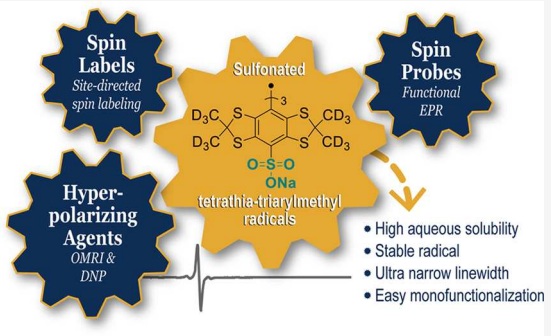

1. INTRODUCTION

Triarylmethyl radicals (TAM, trityl) of type tetrathiatriarylmethyl are unique spin probes and spin labels used for biomedical electron paramagnetic resonance (EPR) applications. These radicals exhibit unmatched properties, such as ultranarrow linewidth, (e.g., <40 mG for deuterated Finland trityl (**dFT**), Figure 1) due to their long relaxation times and exceptional stability within biological media.[1] These features make tetrathiatriarylmethyl radicals superior spin probes and labels by comparison to the commonly used nitroxide radicals. Indeed, the latter being generally hampered by their fast reduction in biological media and their broad linewidths.[2] The most representative structures of tetrathiatriarylmethyl radicals are the Finland trityl (**FT**), **OX063**, and their deuterated analogs (**dFT** and **OX071**)(Figure 1).

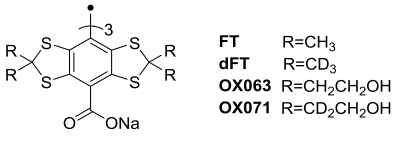

Figure 1. Structure of **FT**, **OX063** radicals, and their deuterated analogs.

Because of their unprecedented properties, tetrathiatriarylmethyl radicals have been widely used as spin probes for *in vivo* low-field EPR to measure the physiologically relevant parameters such as pO_2, pH, and inorganic phosphate concentration [Pi].[3,4] Besides, as spin labels of biomacromolecules, they have enabled distance measurement in DNA and proteins for structural biology studies using dipolar EPR spectroscopy.[5−7] Tetrathiatriarylmethyl radicals are efficient hyperpolarizing agents for dissolution dynamic nuclear polarization (d-DNP)[8,9] and Overhauser-enhanced magnetic resonance imaging (OMRI).[10,11] Very recently, we demonstrated that a tetrathiatriarylmethyl radical-labeled ^{13}C at the central carbon enables the measurement of the probe rotational correlation time with applications to measure microviscosity and molecular dynamics by EPR.[12]

The developments of tetrathiatriarylmethyl radicals relied exclusively on modifications of the Finland trityl but not of the **OX063/71** derivatives.[13−18] This is mostly due to the availability of large-scale chromatographic column-free syntheses of (**d**)**FT**,[19−21] while the syntheses of hydroxyethyl derivatives **OX063/71** are twice longer and have only been reported very recently.[22] Unfortunately, for *in vivo* applications, **FT**-based

Received: March 2, 2020
Published: July 23, 2020

https://dx.doi.org/10.1021/acs.joc.0c00557
J. Org. Chem. 2020, 85, 10388−10398

derivatives show unwanted lipophilic interactions with plasma biomacromolecules, such as albumin, which in turn result in a broadening of the EPR line.[23] Therefore, when injected *in vivo*, only the unbound fraction of **FT**-based TAMs is detected. Also, Finland trityl aggregates at high saline concentration and at low pH.[20] Therefore, a more hydrophilic structure of **FT** would be highly desirable to address these limitations. Hereby, we report on the synthesis, characterization, and application of a highly hydrophilic sulfonated triarylmethyl radical for biomedical EPR applications.

2. EXPERIMENTAL SECTION

2.1. Generals. High-performance liquid chromatography (HPLC) analysis was carried out using a Waters Alliance e2695 separation module, equipped with a 2998 PDA detector and an SQD2 Mass Detector. A XBridge BEH C18 4.6 mm × 50 mm, 2.5 μm column was used for separation with the following conditions: flow rate, 1.5 mL/min; column temperature, 40 °C, gradient, $t_{0\,min}$: H_2O: 80%, ACN: 10%, H_2O with 1% trifluoroacetic acid (TFA): 10%; $t_{5\,min}$: H_2O: 0%, ACN: 90%, H_2O with 1% TFA: 10%; $t_{6\,min}$: H_2O: 0%, ACN: 100%, H_2O with 1% TFA: 0%. High-resolution mass spectra (HRMS) were recorded using a Thermofisher Scientific Q Exactive Mass Spectrometer with an electron spray ionization (ESI) source. CW X-band EPR spectra were recorded using an ELEXSYS E580 EPR spectrometer (Bruker, Germany). For the EPR spectra recorded under a controlled gas composition, the solutions were filled into a gas-permeable Teflon tube (diameter, 1.14 mm, wall thickness, 60 μm, Zeus, Inc.) and a gas flow of a controlled composition was applied using a temperature and gas controller (Noxygen, Germany). The g-factors were determined using **dFT** as an internal standard (g = 2.00307).[24] UV−Vis measurements were performed using an Agilent Carry 60 spectrophotometer. Preparative purification of **dFT-(SO$_3$)$_3$** was carried out using a Teledyne CombiFlash Rf+ purificator and a C18 column. **dFT** and **OX063** radicals were synthesized according to the reported procedures.[20,21,22] 5,5-Dimethyl-1-pyrroline *N*-oxide (**DMPO**) was purchased from Dojindo Molecular Technologies. All other reagents and solvents were purchased from Sigma-Aldrich and Fisher Scientific and used without further purification.

2.2. Chemistry. *2.2.1. dFT in Aerated Na_2SO_3 Solution.* **dFT** was stirred for 2.5 h in aerated aqueous sodium sulfite solution, the final concentrations were 200 μM for **dFT** and 200 mM for sodium sulfite. Then, an aliquot was transferred into a gas-permeable EPR capillary and the EPR spectra were recorded under a constant nitrogen flow and also analyzed by high-performance liquid chromatography-mass spectrometry (HPLC-MS). The EPR acquisition parameters were ModAmp 0.020 G, ModFreq. 10.00 kHz, ConvTime 20.00 ms, power 0.02993 mW, and SweepWidth 2.5 G, 2048 pts.

2.2.2. dFT in the Sulfite Anion Radical ($SO_3^{\bullet-}$) Generating System. Potassium dichromate in water was added to a solution of **dFT** (final concentration = 200 μM) in aqueous sodium sulfite (final concentration = 200 mM) under a nitrogen atmosphere. The final concentrations of $K_2Cr_2O_7$ were 1, 3, 5, 10, and 20 mM. Shortly after mixing, an aliquot was transferred into a gas-permeable EPR capillary, and the EPR spectra were recorded at 37 °C under constant nitrogen flow. In addition, HPLC-MS analyses were performed for [$K_2Cr_2O_7$] = 10 mM after 5 and 90 min. The EPR spectrum was recorded using the following acquisition parameters: ModAmp 0.030 G, ModFreq. 10.00 kHz, ConvTime 20.00 ms, power 0.02993 mW, SweepWidth 2.5 G, 1024 pts. The confirmation of the formation of the sulfite anion radical in the system was verified by spin trapping of $SO_3^{\bullet-}$ using **DMPO**. $K_2Cr_2O_7$ (final concentration = 3 mM) was added to a solution containing **DMPO** (final concentration = 20 mM), **dFT** (final concentration = 200 μM), and sodium sulfite (final concentration = 200 mM) and under a nitrogen atmosphere at room temperature. The EPR spectrum was recorded using the following acquisition parameters: ModAmp 0.7 G, ModFreq. 30.00 kHz, ConvTime 20.00 ms, power 15 mW, SweepWidth 70 G, and 2048 pts.

2.3. Determination of the Rate Constant of the Monosulfonation Reaction. **DMPO** was used as a competitor for the sulfite anion radical. In the presence of a competitor, the generated sulfite anion radical reacts with **DMPO** and **dFT** with second-order rate constants k_1 and k_2, correspondingly.

$$SO_3^{\bullet-} + \text{DMPO} \rightarrow \text{DMPO} - SO_3 \quad k_1$$

$$SO_3^{\bullet-} + \text{dFT} \rightarrow \text{dFT} - (SO_3)_1 \quad k_2$$

With **DMPO**: in the steady-state regime, the rate of generation of sulfite anion radicals, V_{gen}, is equal to its consumption by **dFT** and **DMPO**.

$$0 = V_{gen} - k_1[\text{DMPO}][SO_3^{\bullet-}] - k_2[\text{dFT}][SO_3^{\bullet-}] \quad (1)$$

The steady-state concentration of sulfite anion radical can be derived from eq 1.

$$[SO_3^{\bullet-}] = \frac{V_{gen}}{k_1[\text{DMPO}] + k_2[\text{dFT}]} \quad (2)$$

Using eq 2, the rate of **dFT-(SO$_3$)$_1$** formation in the presence of the competitor, V_{DMPO}, equals

$$\frac{d}{dt}[\text{dFT} - (SO_3)_1] = V_{DMPO} = k_2[\text{dFT}][SO_3^{\bullet-}] = k_2[\text{dFT}]\frac{V_{gen}}{k_1[\text{DMPO}] + k_2[\text{dFT}]} \quad (3)$$

Without **DMPO**: in the steady-state regime, the rate of sulfite anion radical generation equals the rate of **dFT-(SO$_3$)$_1$** formation, $V_{no\ DMPO}$:

$$0 = V_{gen} - k_2[\text{dFT}][SO_3^{\bullet-}] \quad (4)$$

$$\frac{d}{dt}[\text{dFT} - (SO_3)_1] = V_{no\ DMPO} = k_2[\text{dFT}][SO_3^{\bullet-}] \quad (5)$$

$$V_{gen} = k_2[\text{dFT}][SO_3^{\bullet-}] = V_{no\ DMPO} \quad (6)$$

By combining eqs 3 and 6, we can derive the rate of **dFT-(SO$_3$)$_1$** formation in the presence of the **DMPO** competitor:

$$V_{DMPO} = k_2[\text{dFT}]\frac{V_{no\ DMPO}}{k_1[\text{DMPO}] + k_2[\text{dFT}]} \quad (7)$$

The ratio between the rate of **dFT-(SO$_3$)$_1$** formation in the absence and presence of the competitor can be derived from eq 7

$$\frac{V_{no\ DMPO}}{V_{DMPO}} - 1 = \frac{k_1[\text{DMPO}]}{k_2[\text{dFT}]} \quad (8)$$

$K_2Cr_2O_7$ (final concentration = 3 mM) was added to a solution containing **dFT** (final concentration = 200 μM), Na_2SO_3 (final concentration = 200 mM), and **DMPO** (final concentrations = 0, 5, 10, 15, 20 mM) in water under a nitrogen atmosphere at room temperature. The total volume was 100 μL. Immediately after mixing, the solution was filled into a gas-permeable Teflon EPR capillary and placed inside the X-band EPR cavity. A flow of nitrogen was maintained throughout the experiment. The decay of **dFT** concentration was followed for 25 min, corresponding to a maximum of 15% conversion. The **dFT** decay allows to determine $V_{no\ DMPO}$ (0 mM DMPO) and V_{DMPO} (5, 10, 15, 20 mM DMPO). The plot $\frac{V_{no\ DMPO}}{V_{DMPO}} - 1$ vs [DMPO] allows to determine k_2 = 3.53×10^8 M^{-1} s^{-1} using k_1 = 1.2×10^7 M^{-1} s^{-1}.[25] The EPR spectra were recorded using the following acquisition parameters: ModAmp 0.020 G, ModFreq. 10.00 kHz, ConvTime 20.00 ms, power 0.02993 mW, SweepWidth 2.5 G, and 2048 pts.

2.4. EPR Characterization. The anoxic peak-to-peak (ΔB_{pp}) linewidth of **dFT-(SO$_3$)$_3$** was measured from a spectrum of 50 μM in phosphate buffer saline (10 mM, pH = 7.4, NaCl 140 mM) using the following parameters: ModAmp 0.010 G, ModFreq. 10.00 kHz, ConvTime 20.00 ms, power 0.02993 mW, SweepWidth 0.5 G, 1024 pts. For the measurement of the ^{13}C and ^{33}S satellites, an aliquot from the C18 purification was analyzed directly without evaporation of the solvent. The solvent composition was 13% ACN in water containing 0.3% TFA.

https://dx.doi.org/10.1021/acs.joc.0c00557
J. Org. Chem. 2020, 85, 10388−10398

EPR acquisition parameters were ModAmp 0.010 G, ModFreq. 10.00 kHz, ConvTime 20.00 ms, power 0.02993 mW, SweepWidth 18.0 G, and 8192 pts.

2.4.1. Computational Chemistry. The geometry of **dFT-$(SO_3)_3$** was optimized at the UB3LYP/6-31G* level of theory using the ORCA 4.2.0 computational package.[26] The isotropic hyperfine splittings with ^{13}C and ^{33}S were calculated using the "eprnmr" ORCA keyword for a single-point calculation using the IGLO-III basis sets for the optimized geometry. The UB3LYP functional has previously given good predictions of the experimental results for this family of trityl radicals.[27,28] The sulfo groups were treated as protonated rather than sodium salts.

2.5. Interaction With Albumin, Solubility at Low pH, and Stability Under Reducing Environment and in Cell Lysate. To investigate the interaction with albumin, **dFT**, **dFT-$(SO_3)_3$**, and **OX063** (final concentration = 50 μM) were incubated with various concentrations of bovine serum albumin (BSA) (final concentration from 0 to 1 mM) in phosphate buffer saline (10 mM, pH = 7.4, NaCl 140 mM) under a nitrogen atmosphere. To compare TAMs with different intrinsic linewidths, the EPR signal intensities were measured for each BSA concentration and normalized to EPR intensity without BSA ($I_{BSA}/I_{no\ BSA}$). The EPR acquisition parameters were: ModAmp 0.020 G, ModFreq 10.00 kHz, ConvTime 20.00 ms, power 0.02993 mW, SweepWidth 0.5 G, 1024 pts. To investigate the solubility of **dFT-$(SO_3)_3$** at low pH, the EPR spectra of **dFT-$(SO_3)_3$** (100 μM) were recorded at pH 1.1 and 7.4 and the EPR signal intensities were compared. The EPR acquisition parameters were ModAmp 0.100 G, ModFreq 30.00 kHz, ConvTime 40.00 ms, power 0.09464 mW, SweepWidth 5.0 G, and 1024 pts. The stability of **dFT-$(SO_3)_3$** under reducing environment was investigated by mixing **dFT-$(SO_3)_3$** (final concentration = 50 μM) with ascorbate (final concentration = 500 μM) in a mixture with reduced glutathione (final concentration = 650 μM).[29] The EPR time course was recorded under nitrogen flow for half an hour. The EPR acquisition parameters were ModAmp 0.025 G, ModFreq 30.00 kHz, ConvTime 40.00 ms, power 0.09464 mW, SweepWidth 5.0 G, and 1024 pts. The stability in the cell lysate was investigated by incubating **dFT-$(SO_3)_3$**, **dFT**, and **OX063** (200 μM) with the MDA-MB-231 cell lysate at 37 °C under a nitrogen atmosphere for 30 min. Briefly, 2×10^7 MDA-MB-231 cells grown in Dulbecco's modified Eagle's medium (DMEM) supplemented with 10% fetal bovine serum (FBS) were mechanically collected by scraping in phosphate-buffered saline (PBS) and subsequently centrifuged at 450 rcf for 5 min at 4 °C to pellet the cells. The packed cell volume of the cells was about 75 μL. The cells were resuspended in 500 μL of ice-cold lysis buffer (25 mM Tris-HCl, pH 7.4, 150 mM NaCl, 1% NP-40 (IGEPAL CA630), 1 mM ethylenediaminetetraacetic acid (EDTA), 1.5 mM $MgCl_2$, 5% glycerol, and Halt protease inhibitor cocktail (Pierce)) and incubated on ice for 30 min. The lysate was clarified by centrifugation at 20.000 rcf for 10 min at 4 °C and the supernatant was collected. One microlitre of a 10 mM stock solution of **dFT-$(SO_3)_3$**, **dFT**, or **OX063** was added to 49 μL of the cell lysate. The mixture was filled into a gas-permeable Teflon EPR capillary and placed inside the X-band EPR cavity and EPR time courses were recorded under nitrogen flow for half an hour at 37 °C. The EPR acquisition parameters were ModAmp 0.030 G, ModFreq 30.00 kHz, ConvTime 30.00 ms, Power 0.09464 mW, SweepWidth 5.0 G, and 1024 pts.

2.6. Oxygen Sensitivity and *In Vivo* Oxygen Imaging. To determine the oxygen sensitivity, **dFT-$(SO_3)_3$** (50 μM) in phosphate buffer saline (10 mM, pH = 7.4, NaCl 140 mM) was filled into a gas-permeable Teflon tube and placed in the EPR cavity. The EPR spectra were recorded under various oxygen/nitrogen ratios. The peak-to-peak linewidths were measured for pO_2 = 0, 34.2, 76, 114, and 152 mmHg. The EPR acquisition parameters were ModAmp 0.015 G, ModFreq. 30.00 kHz, ConvTime 40.00 ms, power 0.09464 mW, SweepWidth 3.0 G, and 1024 pts.

2.6.1. In Vivo Oxygen Mapping. Animal studies were performed according to the approved WVU Institutional Animal Care and Use Committee (IACUC) protocol.

5×10^5 C57Bl/6J PyMT mouse breast tumor cells (ATCC CRL-3278) were orthotopically implanted into the number 4 abdominal mammary glands of the female C57Bl/6J mice. Tumor volumes were determined using calipers measuring the shortest and perpendicular longest dimensions. The tumor oxygen was imaged when the tumor reached a volume of approximately 257 mm^3 using the equation $V = 0.5x$ (shortest dimension^2 × longest dimension). Briefly, 50 μL of a 2 mM solution of sulfonated trityl radical **dFT-$(SO_3)_3$** in 10 mM phosphate buffer saline was injected intratumorally in an anesthetized mouse. Immediately after, the animal was placed in a custom-built Rapid-Scan EPR imager operating at 800 MHz.[30] Acquisition parameters were as follows: rapid-scan frequency, 9.4 kHz; number of projections, 2546; maximum gradient, 3 G/cm; acquisition time, and 8.25 min. An integral intensity threshold of 30% was implemented to remove low signal-to-noise data.

2.7. Generation of the Trisulfonated TAM Cation and *Ipso*-Substitution by S-, N-, and P-Nucleophiles. The stability of the **dFT-$(SO_3)_3$** cation was investigated by UV−visible spectroscopy. A quartz cuvette was filled with **dFT-$(SO_3)_3$** in phosphate buffer (100 mM, pH = 7.4) at room temperature, and then, 1 equiv of K_2IrCl_6 was added. Immediately after mixing, the spectra were recorded every 1 min for 10 min. The total volume was 3 mL, and the final concentrations of **dFT-$(SO_3)_3$** and K_2IrCl_6 were 50 μM.

Scheme 1. Unsuccessful Attempt of the Synthesis of Sulfonated Trityl 3

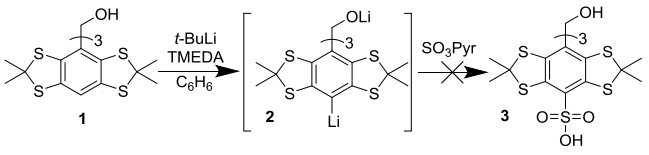

3. RESULTS AND DISCUSSION

3.1. Synthesis. To overcome the issue arising from the lipophilicity of Finland trityl, we sought to substitute the three carboxyl groups by a more hydrophilic moiety, which does not give rise to an additional hyperfine splitting in the EPR spectrum. The sulfo

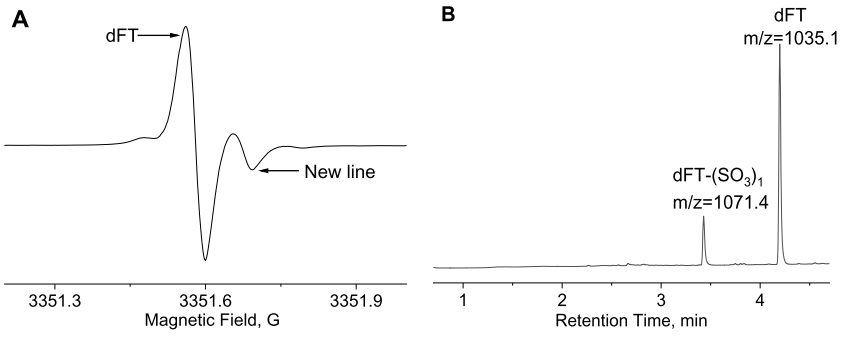

Figure 2. (A) EPR spectrum of the **dFT** radical (200 μM) in aerated sodium sulfite (200 mM) after stirring for 2.5 h. (B) Reverse-phase HPLC-MS chromatogram of the **dFT** radical under the same conditions.

https://dx.doi.org/10.1021/acs.joc.0c00557
J. Org. Chem. 2020, 85, 10388−10398

functional group seemed to be the ideal candidate to meet these requirements. Our first attempt to introduce the sulfo group through a classical addition of the aryllithium **2**, generated from the deprotonation of **1** with *tert*-butyl lithium, to sulfur trioxide pyridine complex (Scheme 1) failed to provide the desired compound **3**, as a complex mixture was obtained.

Serendipitously, we noticed that a solution of deuterated Finland trityl (**dFT**) (200 μM) in aerated sodium sulfite (200 mM) stirred for 2.5 h yielded to the formation of a new EPR line observed at X-band (Figure 2A). The HPLC-MS analysis of the mixture revealed the presence of 17% of a new peak with a retention time (RT) of 3.4 min and a molecular weight (m/z = 1071.4) before the peak of **dFT** (RT = 4.1 min, m/z = 1035.1), consistent with the substitution of one carboxyl group by a sulfo group (Figures 2B and S1). The same reaction carried out under strictly deoxygenated conditions did not result in the formation of this new compound (data not shown).

By analogy with the sequential substitution of the carboxyl groups of **dFT** by a nitro group with $NO_2^{\bullet}$ described previously,[17,31] we hypothesized that the monosulfonated TAM resulted from the reaction of **dFT** with the sulfite anion radical ($SO_3^{\bullet-}$) generated in aerated sodium sulfite solutions. To drive further the reaction, we incubated **dFT** (200 μM) in a sulfite anion radical generating system composed of sodium sulfite (200 mM) and potassium dichromate (from 1 to 20 mM) under a nitrogen atmosphere. The reactions were monitored by X-band EPR and HPLC-MS. The EPR spectra (Figure 3A) show the conversion of the single EPR line of **dFT** to three new lines at higher magnetic fields with different *g*-factors (Table S1). At a high concentration of potassium dichromate (20 mM), we observed a fast conversion of **dFT** EPR line to the line at the highest magnetic field. The HPLC-MS chromatograms show similar results (Figures 3B and S2), the **dFT** peak (RT = 4.1 min, m/z = 1035.1) was progressively converted to three more polar compounds with peaks (RT_1 = 3.4 min, m/z = 1071.4; RT_2 = 2.6 min, m/z = 1107.3, RT_3 = 1.8 min, m/z = 1144.3) corresponding to the mono-, di-, and trisulfonated TAM (Figure 3C) as determined by their mass spectra.

To verify that the sulfite anion radical was generated in this system, a solution of **dFT** (200 μM) was incubated with Na_2SO_3 (200 mM) and $K_2Cr_2O_7$ (3 mM) in the presence of the **DMPO** (20 mM) spin trap at room temperature under nitrogen. The EPR spectrum showed the formation of the characteristic **DMPO-SO_3** nitroxide adduct[32] (Figure S3), confirming the formation of the sulfite anion radical. Based on this result, our proposed mechanism involves the addition of the sulfite radical at the parapposition of the aryl ring, which triggers an oxidative decarboxylation as reported previously for the substitution of the carboxyl moieties of Finland trityl by nitro groups with $NO_2^{\bullet}$ (Scheme 2).[17,31]

The reaction was easily scaled up to 1 g without any difficulty, allowing to isolate the trisulfonated TAM in 95% yield after purification using a C18 column (see the Supporting Information for detailed procedure).

3.2. Determination of the Rate Constant. To determine the rate constant of the reaction between **dFT** and the sulfite anion radical, the competition kinetics method was used with **DMPO** as a competitor (Figure 4A). To isolate the first step of the reaction (monosulfonation), the reactions were monitored by EPR to a maximum of 15% conversion of **dFT**, which does not result in the formation of the disulfonated trityl radical (**dFT-$(SO_3)_2$**). The reactions were performed with various **DMPO** concentrations (0, 5, 10, 15, 20 mM) and the initial rates were determined for each kinetics (Figure 4B). The rate ratio

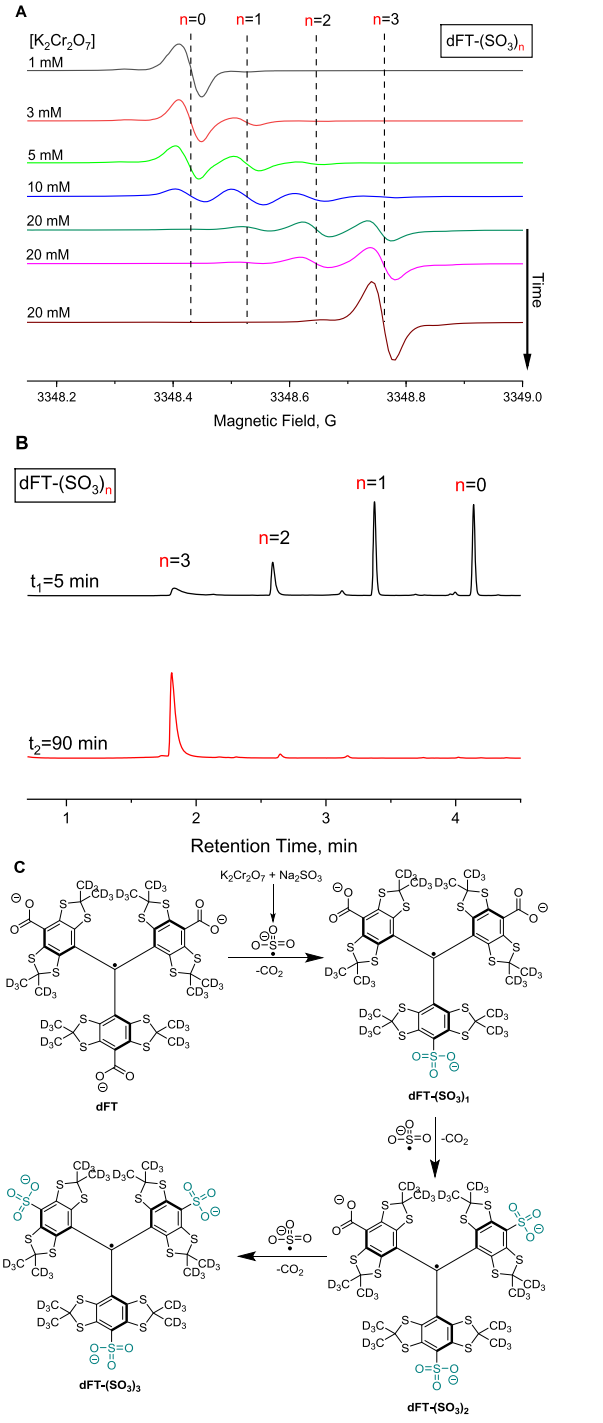

Figure 3. (A) X-band EPR of the **dFT** (200 μM) in sodium sulfite (200 mM) in the presence of various concentrations of potassium dichromate (1, 3, 5, 10, 20 mM) at 37 °C under a nitrogen atmosphere showing the sequential sulfonation of the **dFT** radical into the trisulfonated TAM radical. (B) Reverse-phase HPLC-MS of a solution containing **dFT** (200 μM) in sodium sulfite (200 mM) and in potassium dichromate (10 mM) under a nitrogen atmosphere after 5 and 90 min. (C) Chemical scheme of the sequential sulfonation of the **dFT** radical into the trisulfonated **dFT** radical.

without and with the competitor allows to determine the second-order rate constant of the reaction, which equals 3.53 × 10^8 M^{-1} s^{-1} (Figure 4C). It is worth noting that such a high rate constant will allow further applications of **dFT** to trap the sulfite anion radicals with EPR or HPLC detection.[32,33]

https://dx.doi.org/10.1021/acs.joc.0c00557
J. Org. Chem. 2020, 85, 10388−10398

Scheme 2. Proposed Mechanism for the Substitution of the Carboxyl Moieties of dFT by the Sulfo Groups

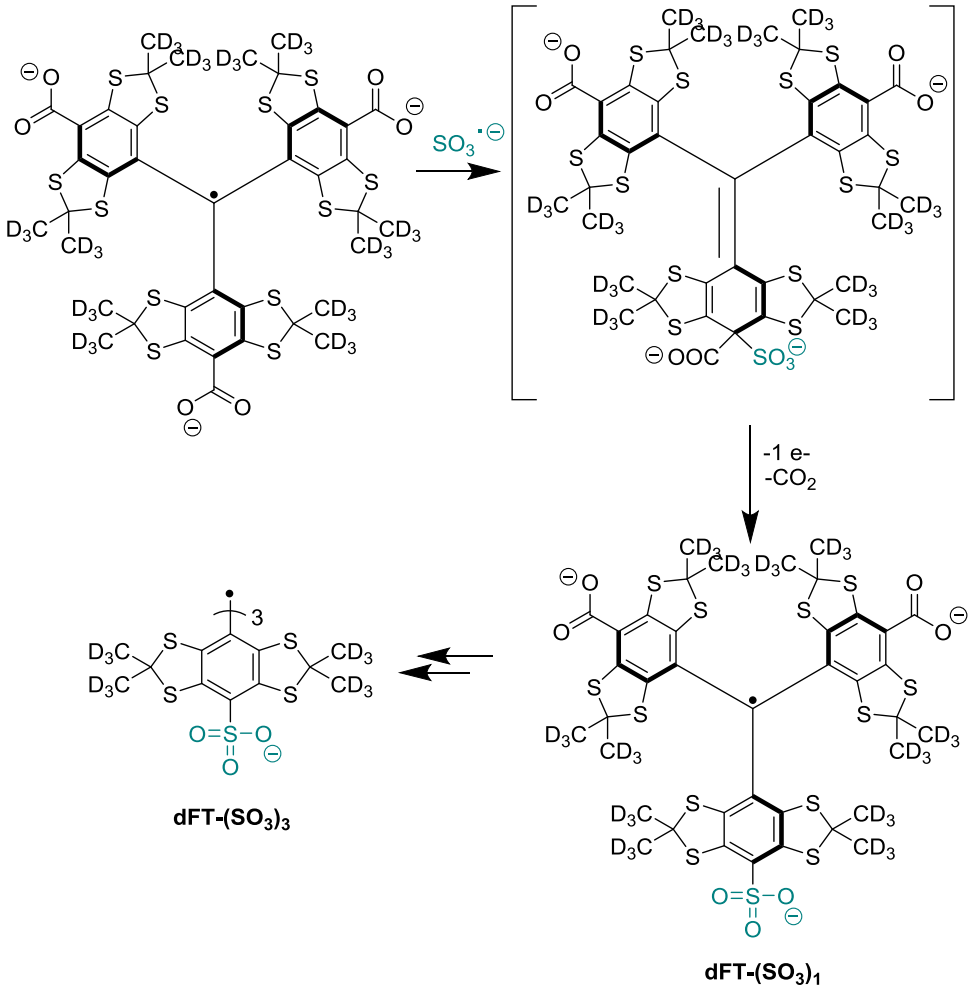

3.3. EPR Spectrum. The EPR spectrum of **dFT-$(SO_3)_3$** (50 μM) in phosphate buffer saline (10 mM, pH = 7.4, NaCl 140 mM) recorded at X-band under a nitrogen atmosphere shows a single line with an ultranarrow peak-to-peak linewidth of ΔB_{pp} = 24 mG (Figure 5A). To our knowledge, this is the narrowest linewidth of all TAMs reported to date. A narrow linewidth leads to a high-intensity signal, which is of first importance for *in vivo* applications where the signal-to-noise ratio (SNR) is always a critical issue. Also, the spectrum shows additional low-intensity peaks corresponding to the ^{13}C satellites (the ^{13}C natural abundance is 1.1%, I = 1/2) of the aryl rings (Figure 5B). The values of all ^{13}C hyperfine splitting constants (hfs) show high similarity with those reported for **dFT** (Table 1). Interestingly, a quartet: 1:1:1:1 resulting from the interaction between the free electron with the three ^{33}S (the ^{33}S abundance is 0.75%, I = 3/2) of the sulfo groups is also visible (Figure 5B, red dots). To confirm the attribution of this quartet to the ^{33}S of the sulfo groups, we computed the hfs using density functional theory calculations. First, the geometry of **dFT-$(SO_3)_3$** was optimized at the UB3LYP/6-31G* level of theory (Figure S4). Then, we performed a single-point calculation using IGLO-III basis set to compute the isotropic hfs. The measured hfs = 0.65 G is in good agreement with the value calculated: −0.70 G. Note that the measurements were performed using CW EPR, which does not allow to determine the sign of the hfs. In addition, all calculated ^{13}C satellites hfs are in good agreement with the measured hfs. Notably, similar small ^{33}S coupling was not observed for a sulfonated perchlorinated TAM because of its ∼30 times larger linewidth compared to **dFT-$(SO_3)_3$**.[34]

3.4. Interaction With Albumin, Solubility at Low pH, and Stability under Reducing Environment and in the Cell Lysate. To investigate whether the substitution of the three carboxyl groups of **dFT** by the sulfo groups decreases the interaction with albumin, the EPR spectra of **dFT** and **dFT-$(SO_3)_3$** in the presence of various concentrations of bovine serum albumin (BSA) were recorded (Figure 6). While **dFT** loses 80% of its EPR signal intensity upon incubation with 1 equiv (BSA) due to a line broadening, indicating a strong interaction,[23] **dFT-$(SO_3)_3$** loses less than 25% showing a lower affinity to albumin. This result can be explained by the higher hydrophilicity of the sulfo group in comparison to the carboxyl moiety. Conversely, the EPR intensity of **OX063** recorded under the same conditions did not change upon incubation with BSA, showing the total absence of interaction with albumin. Spin labels based on **FT** have shown unwanted nonspecific bindings to the hydrophobic sites of proteins and membranes.[23,35] **OX063/71** are more hydrophilic but have slightly larger molecular volumes (50% larger molecular volumes, considering radii of 7 and 8 Å for **dFT-$(SO_3)_3$** and **OX063/71**,[3636] respectively), which could interfere with the structure of the macromolecule under investigation. **dFT-$(SO_3)_3$** has the advantage of high hydrophilicity without increasing the size of the label.

The protonation of the carboxyl groups of **dFT** is responsible for its aggregation at pH lower than 5.[20] The substitution of the

https://dx.doi.org/10.1021/acs.joc.0c00557
J. Org. Chem. 2020, 85, 10388−10398

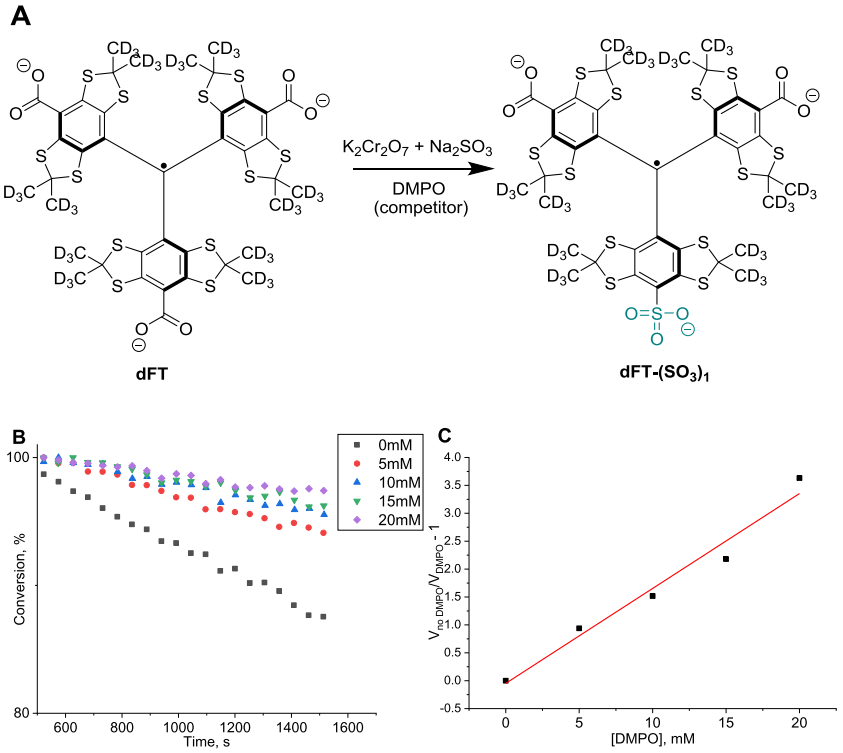

Figure 4. (A) Scheme of the reaction of **dFT** with $SO_3^{\bullet-}$ in the presence of **DMPO** as a competitor. (B) Initial rates of the reaction with various concentrations of **DMPO** (0, 5, 10, 15, 20 mM). (C) Rate ratio without and with various concentrations of **DMPO** allowing to determine the rate constant of 3.53×10^8 M^{-1} s^{-1} for the monosulfonation reaction.

carboxyl functions by the sulfo groups, with a $pK_a < 0$ keep the molecule charged at any physiological pH, prevents this aggregation. Indeed, no change in the EPR signal intensity was observed between the spectra of **dFT-$(SO_3)_3$** (100 μM) recorded at pH 7.4 and 1.1 (data not shown). Importantly, the introduction of three sulfo-withdrawing groups does not result in an instability toward biologically relevant reducing agents. Indeed, **dFT-$(SO_3)_3$** (50 μM) incubated in the presence of an excess of ascorbic acid (500 μM) in mixture with glutathione (GSH) (650 μM)[29] for more than 30 min under a nitrogen atmosphere did not result in a noticeable decrease of the EPR signal intensity, demonstrating its stability toward those biological reducing agents (Figure S5A). Note that this result contrast with the fast reduction by ascorbic acid observed for a sulfonated perchlorinated TAM.[34] Also, **dFT-$(SO_3)_3$** (200 μM) incubated with the lysate of the MDA-MB-231 triple-negative breast cancer cell line for 30 min under a nitrogen atmosphere at 37 °C resulted in less than 3% decrease of the EPR signal intensity (Figure S5B). Similar results were obtained with **OX063** with 1% decay, while **dFT** decayed by 9% under the same conditions (Figure S5B).

3.5. Oxygen Sensitivity and EPR Imaging of Tumor Oxygenation *In Vivo*. While molecular oxygen is a paramagnetic substance, it cannot be measured directly in solution by EPR due to its fast relaxation times. However, the Heisenberg spin exchange between dissolved molecular oxygen and a free radical such as a TAM or a nitroxide results in a broadening of the EPR linewidth of the radicals.[2,37] This effect can be used to measure oxygen concentration, including *in vivo*.[2] Comparing to nitroxides, tetrathiatriarylmethyl radicals show a higher sensitivity to oxygen due to 1 order of magnitude smaller anoxic linewidth (typically ~100 mG vs ~1 G for nitroxides), resulting in a relative larger linewidth variation.[2,37] The EPR spectra of **dFT-$(SO_3)_3$** (50 μM) in PBS were recorded with different oxygen partial pressures (pO_2) allowing to determine an oxygen peak-to-peak linewidth broadening of 0.52 mG/mmHg pO_2 (Figure 7). This sensitivity is similar to the 0.53 mG/mmHg pO_2 previously reported for **dFT**,[38] demonstrating that **dFT-$(SO_3)_3$** can be used as an oximetric spin probe.

To demonstrate the application of **dFT-$(SO_3)_3$** for EPR oximetry *in vivo*, we performed 4D spectral-spatial imaging (3D-spatial, 1D-spectral) in a breast cancer tumor of an MMTV-PyMT mouse model using a home-build 800 MHz EPR rapid-scan imager; the linewidth in each voxel allows for pO_2 mapping. Figure 8A shows the oxygen distribution in a slice of the tumor in the *x,z*-plane. Figure 8B shows the histogram of pO_2 for the entire image. The pO_2 values extracted are consistent with those previously reported in the literature for the same tumor model.[4]

3.6. Generation of the Trisulfonated TAM Cation and *Ipso*-Substitution by S-, N-, and P-Nucleophiles. The ability to replace selectively one sulfo group by a different functional group would expand the applications of the sulfonated tetrathiatriarylmethyl radicals for biomedical EPR applications. Previously, an *Ipso*-nucleophilic substitution of one carboxyl or hydrogen of Finland trityl derivatives by various nucleophiles was reported.[17,39,40] This strategy is based on the reaction of the trityl cation, generated *in situ*, with S-, N-, and P-nucleophiles. We investigated whether a similar strategy could be applied to **dFT-$(SO_3)_3$**. First, **dFT-$(SO_3)_3$** (50 μM) was oxidized to its cation using 1 equiv of the Ir(IV) water-soluble oxidizing agent K_2IrCl_6 (50 μM) in 100 mM phosphate buffer (Figure 9A), this transformation is accompanied by a decrease of the radical UV–Vis absorption peak at λ = 465 nm and an increase of a peak at λ = 790 nm, corresponding to the trityl cation[41] (data not shown). If no nucleophile is added, a water molecule can add at the paraposition of the aryl group (Figure 9A, step 2), leading to **4**, which undergoes an oxidative desulfonation yielding the phenol

https://dx.doi.org/10.1021/acs.joc.0c00557
J. Org. Chem. 2020, 85, 10388–10398

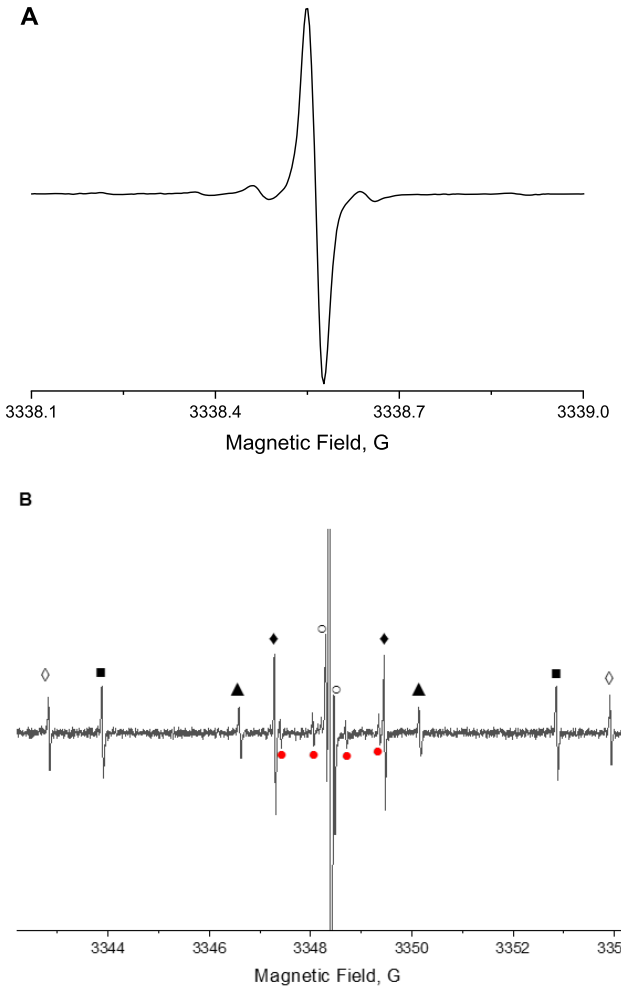

Figure 5. (A) X-band EPR spectrum of **dFT-$(SO_3)_3$** (50 μM) in phosphate buffer saline (10 mM, pH = 7.4, NaCl 140 mM) under a nitrogen atmosphere. (B) Spectrum with 18 G sweep width zoomed on the ^{13}C and ^{33}S satellites.

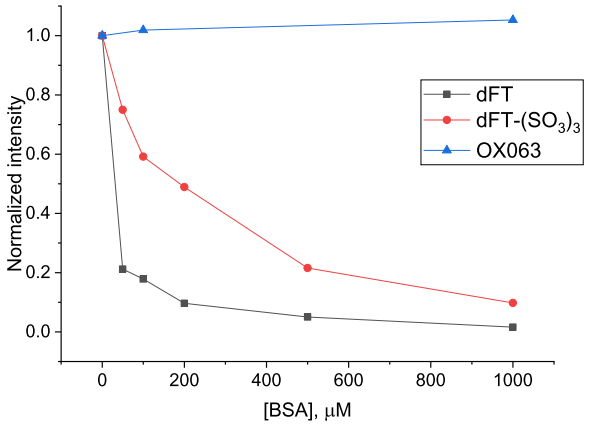

Figure 6. Normalized intensity of the EPR signal of **dFT**, **dFT-$(SO_3)_3$**, and **OX063** (50 μM) in phosphate buffer saline (10 mM, pH = 7.4, NaCl 140 mM) upon incubation with various concentrations of BSA (0–1 mM).

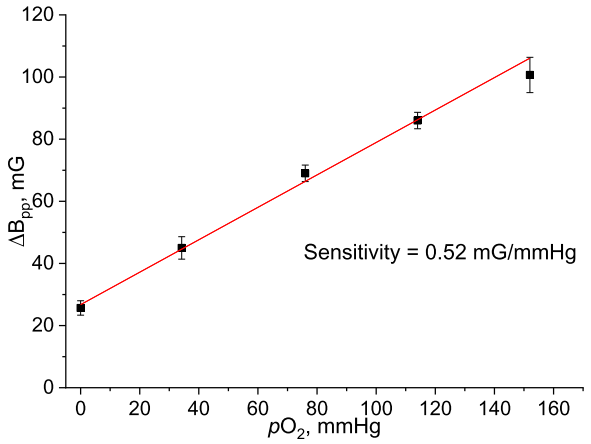

Figure 7. X-band calibration curve of the peak-to-peak linewidth of **dFT-$(SO_3)_3$** (50 μM) in phosphate buffer saline (10 mM, pH = 7.4, NaCl 140 mM) at room temperature with respect to pO_2 leading to a sensitivity of 0.52 mG/mmHg.

5, which in turn is further oxidized to the quinone methide **QM** with a UV–Vis absorption peak at λ = 520 nm (Figure 9B).[17,41] The half-life of the trityl cation was estimated to be 2 min in phosphate buffer pH = 7.4 at room temperature (Figure 9B). Monitored by UV–Vis, the decay of the trityl cation peak at λ = 790 nm is accompanied by an increase of the two peaks, one at λ = 465 nm and the other one at λ = 520 nm corresponding to the trityl radical and **QM**, respectively.[41] The formation of **QM** involves 2 oxidation steps, the HPLC-MS analysis at the end of the reaction shows a ~2:1 ratio between **dFT-$(SO_3)_3$** radical and **QM** (m/z = 1079.1) (data not shown). The presence of **dFT-$(SO_3)_3$** radical that was generated back from the cation indicates that the trityl cation is the oxidant for the steps 3 and 4 in Figure 9.

To investigate whether a strong nucleophile can outcompete the addition of water on the trityl cation, various nucleophiles (20 equiv) were added immediately after the oxidation of the radical. Gratifyingly, we found that S-, N-, and P-nucleophiles

Table 1. Experimental and Calculated hfs Values for ^{13}C and ^{33}S Satellites

	hyperfine splitting, G				
	experimental[a]		calculated[b]		
nucleus (spin)	Finland trityl[c]	**dFT-$(SO_3)_3$**	**dFT-$(SO_3)_3$**	degeneracy	assignment
^{33}S (3/2)	N.A.	0.65	−0.70	3	red circle solid: sulfonate
^{13}C (1/2)	0.18	0.18	−0.27	6	○: thio-ketal
^{13}C (1/2)	2.35	2.18	−2.28	6	◆: 3,5-phenyl
^{13}C (1/2)	3.36	3.58	3.47	3	▲: 4-phenyl
^{13}C (1/2)	9.03	9.00	9.77	6	■: 2,6-phenyl
^{13}C (1/2)	11.46	11.10	−11.41	3	◇: 1-phenyl

[a]The measurements were performed using CW EPR, which does not allow to determine the sign of the hfs. [b]Calculated at the UB3LYP/IGLO-III//UB3LYP/6-31G* level of theory. [c]Converted from the values in MHz measured at 250 MHz.[27]

https://dx.doi.org/10.1021/acs.joc.0c00557
J. Org. Chem. 2020, 85, 10388–10398

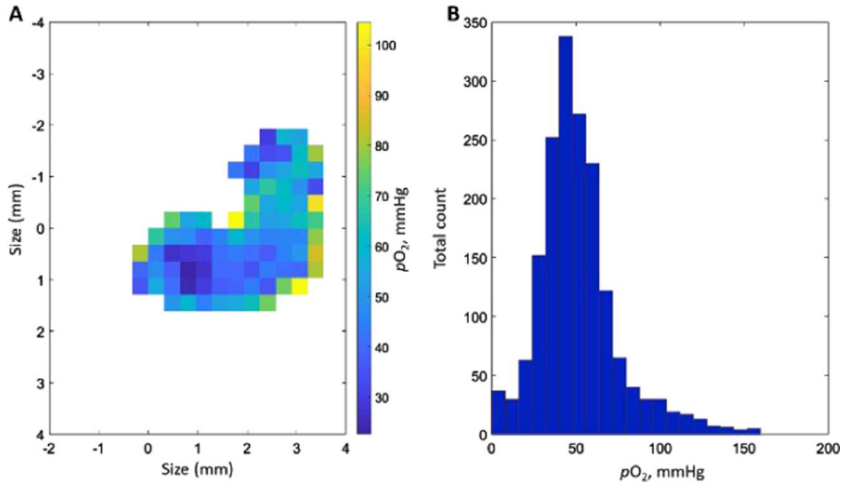

Figure 8. (A) *In vivo* 4D spectral-spatial imaging (3D-spatial, 1D-spectral) in an MMTV-PyMT mouse model of breast cancer. A slice of oxygen distribution in the *x*,*z*-plane is represented. (B) Histogram of oxygen pO_2 distribution for the whole image.

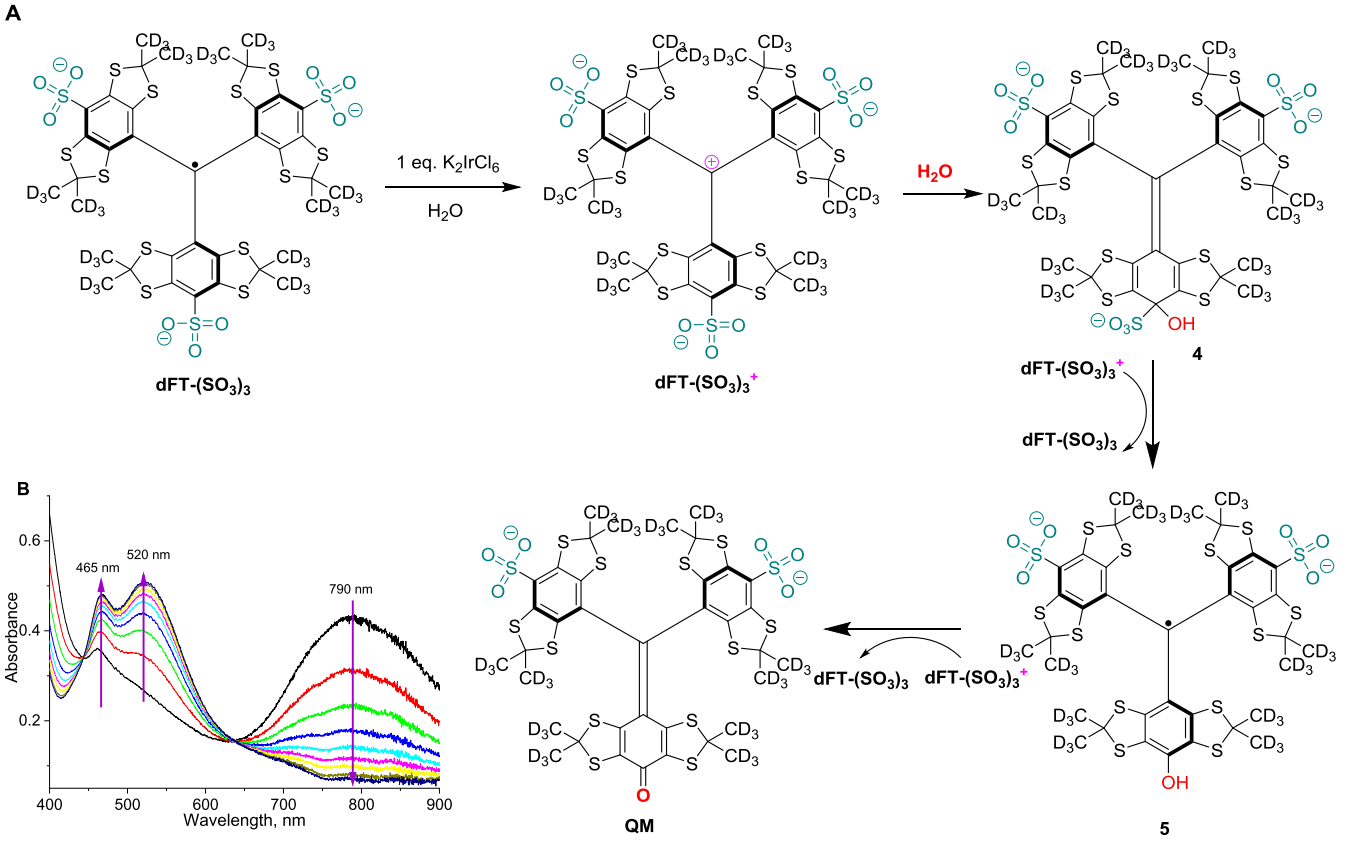

Figure 9. (A) Oxidation of **dFT-$(SO_3)_3$** (50 μM) in phosphate buffer (100 mM, pH = 7.4) at room temperature with K_2IrCl_6 (50 μM) and conversion to **QM**. (B) 10 min time course of the UV−Vis spectra of the conversion of trityl cation (50 μM) to **QM** and **dFT-$(SO_3)_3$**.

such as glutathione (GSH), dimethylamine ($NH(CH_3)_2$), tri-*n*-butylphosphine ($P(n\text{-}Bu)_3$), or trimethylphosphite ($P(OMe)_3$) were able to yield the monofunctionalized sulfonated trityl radicals (Figure 10A). Note that the trimethylphosphite leads to the monodimethylphosphonic ester derivative. The EPR spectra and the HRMS of the purified compounds were in agreement with their molecular structure (Figures 10B and S7−S10); the hyperfine splitting constants were obtained from the simulations (Figure S11). Notably, the mono-GSH derivative **6** exists in a 50:50 mixture of two diastereoisomers arising from the chirality of the trityl core (M, P propeller conformations)[28,42] and L-glutathione. Note that the EPR spectrum of **6** reveals a conjugation through the thiol, as the amine would give an additional hyperfine splitting to the nitrogen nucleus ($I_N = 1$). The monosubstitution of **dFT-$(SO_3)_3$** will allow for the selective synthesis of the unsymmetrical sulfonated trityl radicals with numerous functionalities.

4. CONCLUSIONS

In conclusion, we have shown that the sulfite anion radical substitutes the carboxyl groups of Finland trityl with a high rate constant leading to the highly hydrophilic trisulfonated TAM

https://dx.doi.org/10.1021/acs.joc.0c00557
J. Org. Chem. 2020, 85, 10388−10398

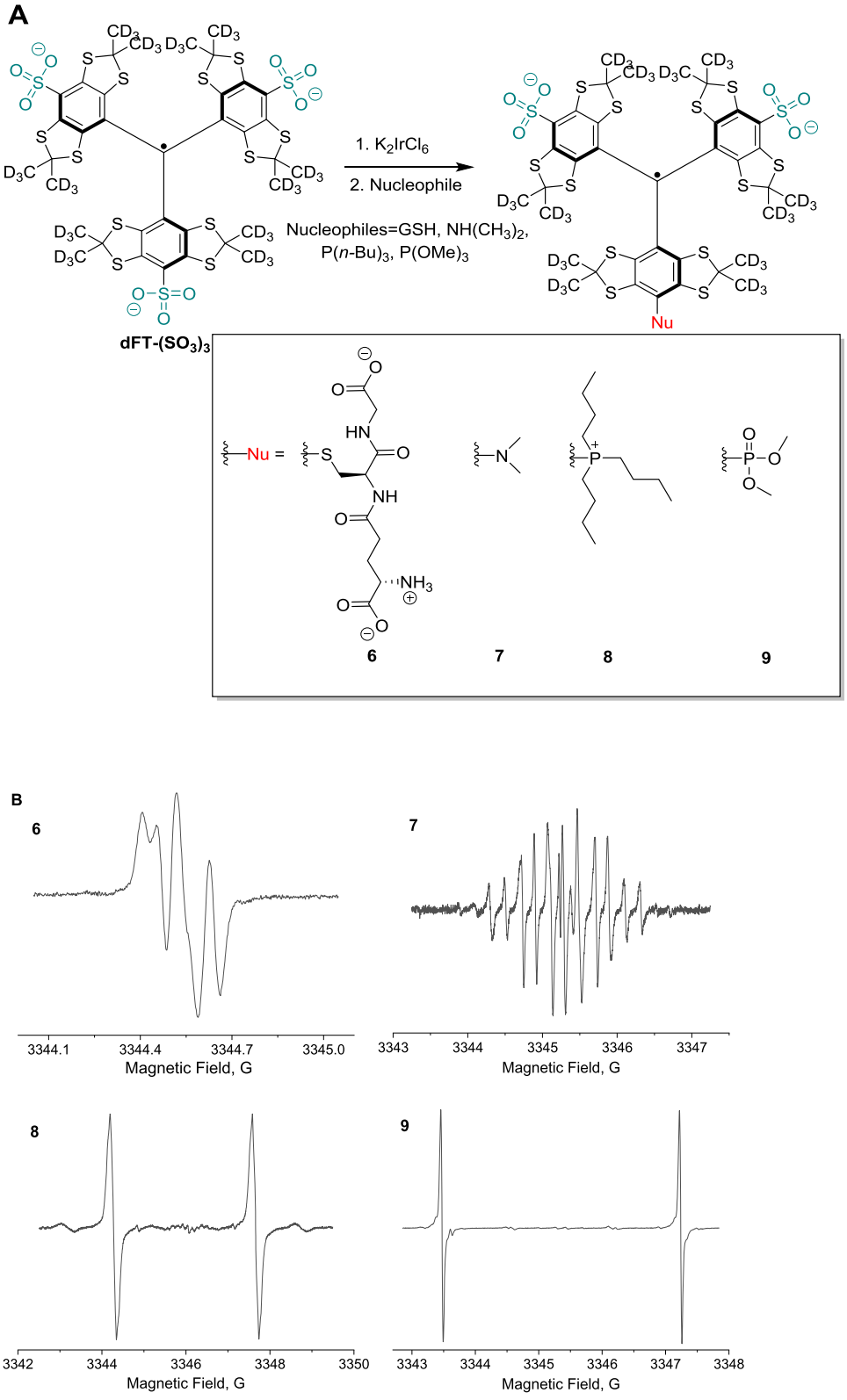

Figure 10. (A) *Ipso*-nucleophilic substitution of **dFT-$(SO_3)_3$** with glutathione (GSH), dimethylamine ($NH(CH_3)_2$), tri-*n*-butylphosphine ($P(n\text{-}Bu)_3$), or trimethylphosphite ($P(OMe)_3$) nucleophiles. (B) X-band EPR spectra of the monofunctionalized sulfonated trityl. hfs obtained from simulations: for **6** (GSH) diastereoisomer 1: a_{H1}=0.03 G, a_{H2}=0.10 G; diastereoisomer 2: a_{H1} = 0.06 G, a_{H2} = 0.10 G; for **7** a_N = 0.18 G, $a_H(6)$ = 0.40 G; for **8** a_P= 3.38 G, $a_H(6)$ = 0.05 G; and for **9** a_P = 3.77 G.

probe, **dFT-$(SO_3)_3$**, showing an ultranarrow linewidth and a lower affinity toward albumin than Finland trityl. We demonstrated the application of **dFT-$(SO_3)_3$** for mapping oxygen concentration *in vivo* in a mouse model of breast cancer. Moreover, we showed the **dFT-$(SO_3)_3$** can be selectively monofunctionalized allowing to expand its applications for biomedical EPR. Our work will enable the synthesis of new sulfonated TAM spin probes, such as a monophosphonated derivative for concurrent

https://dx.doi.org/10.1021/acs.joc.0c00557
J. Org. Chem. 2020, 85, 10388−10398

pO_2, pH, and [Pi] measurements or methanethiosulfonate (MTS), maleimide spin labels for distance measurement in biomacromolecules using dipolar EPR spectroscopy.

■ ASSOCIATED CONTENT

Supporting Information

The Supporting Information is available free of charge at https://pubs.acs.org/doi/10.1021/acs.joc.0c00557.

MS spectra, spin trapping figure, cartesian coordinates for the optimized structure of **dFT-$(SO_3)_3$**, *g*-values, detailed synthetic protocols, and spectral simulations (PDF)

■ AUTHOR INFORMATION

Corresponding Author

Benoit Driesschaert − *In Vivo Multifunctional Magnetic Resonance Center, Robert C. Byrd Health Sciences Center, West Virginia University, Morgantown, West Virginia 26506, United States; Department of Pharmaceutical Sciences, West Virginia University, School of Pharmacy, Morgantown, West Virginia 26506, United States;* orcid.org/0000-0002-1402-413X; Email: benoit.driesschaert@hsc.wvu.edu

Authors

Urikhan Sanzhaeva − *In Vivo Multifunctional Magnetic Resonance Center, Robert C. Byrd Health Sciences Center, West Virginia University, Morgantown, West Virginia 26506, United States; Department of Biochemistry, West Virginia University, School of Medicine, Morgantown, West Virginia 26506, United States*

Martin Poncelet − *In Vivo Multifunctional Magnetic Resonance Center, Robert C. Byrd Health Sciences Center, West Virginia University, Morgantown, West Virginia 26506, United States; Department of Pharmaceutical Sciences, West Virginia University, School of Pharmacy, Morgantown, West Virginia 26506, United States*

Oxana Tseytlin − *In Vivo Multifunctional Magnetic Resonance Center, Robert C. Byrd Health Sciences Center, West Virginia University, Morgantown, West Virginia 26506, United States; Department of Biochemistry, West Virginia University, School of Medicine, Morgantown, West Virginia 26506, United States*

Mark Tseytlin − *In Vivo Multifunctional Magnetic Resonance Center, Robert C. Byrd Health Sciences Center, West Virginia University, Morgantown, West Virginia 26506, United States; Department of Biochemistry, West Virginia University, School of Medicine, Morgantown, West Virginia 26506, United States*

Marieta Gencheva − *In Vivo Multifunctional Magnetic Resonance Center, Robert C. Byrd Health Sciences Center, West Virginia University, Morgantown, West Virginia 26506, United States; Department of Microbiology, Immunology, and Cell Biology, West Virginia University, School of Medicine, Morgantown, West Virginia 26506, United States*

Timothy D. Eubank − *In Vivo Multifunctional Magnetic Resonance Center, Robert C. Byrd Health Sciences Center, West Virginia University, Morgantown, West Virginia 26506, United States; Department of Microbiology, Immunology, and Cell Biology, West Virginia University, School of Medicine, Morgantown, West Virginia 26506, United States*

Valery V. Khramtsov − *In Vivo Multifunctional Magnetic Resonance Center, Robert C. Byrd Health Sciences Center, West Virginia University, Morgantown, West Virginia 26506, United States; Department of Biochemistry, West Virginia University, School of Medicine, Morgantown, West Virginia 26506, United States;* orcid.org/0000-0001-6187-5546

Complete contact information is available at: https://pubs.acs.org/10.1021/acs.joc.0c00557

Author Contributions

All authors have given approval to the final version of the manuscript. U.S. collected and analyzed most of the data, wrote the manuscript. M.P. synthesized the **dFT** and **OX063** radicals, O.T. and M.T. collected and analyzed the *in vivo* oxygen imaging data, and M.G. and M.P. performed the experiments with the cell lysate. T.D.E. oversaw the animal experiments, V.V.K. discussed the kinetic experiments, B.D. conceived the idea, oversaw the project, collected data, and wrote the manuscript. All authors edited the manuscript.

Funding

This work was partially supported by NIH grants (USA): EB023990, CA194013, CA192064, and EB023888. The content is solely the responsibilities of the authors and does not necessarily represent the official view of NIH. West Virginia University Health Sciences Center is acknowledged for its start-up fund to B.D.

Notes

The authors declare no competing financial interest.

■ ACKNOWLEDGMENTS

The authors acknowledge use of the WVU Shared Research Facilities.

■ ABBREVIATIONS

EPR, electron paramagnetic resonance; FT, Finland trityl; TAM, triarylmethyl; OMRI, Overhauser-enhanced magnetic resonance imaging; DMPO, 5,5-dimethyl-1-pyrroline *N*-oxide; hfs, hyperfine splitting; BSA, bovine serum albumin; QM, quinone methide; GSH, glutathione; TFA, trifluoroacetic acid; ACN, acetonitrile; FBS, fetal bovine serum

■ REFERENCES

(1) Ardenkjær-Larsen, J. H.; Laursen, I.; Leunbach, I.; Ehnholm, G.; Wistrand, L. G.; Petersson, J. S.; Golman, K. EPR and DNP Properties of Certain Novel Single Electron Contrast Agents Intended for Oximetric Imaging. *J. Magn. Reson.* **1998**, *133*, 1−12.

(2) Gallez, B.; Baudelet, C.; Jordan, B. F. Assessment of tumor oxygenation by electron paramagnetic resonance: principles and applications. *NMR Biomed.* **2004**, *17*, 240−262.

(3) Marchand, V.; Levêque, P.; Driesschaert, B.; Marchand-Brynaert, J.; Gallez, B. In vivo EPR extracellular pH-metry in tumors using a triphosphonated trityl radical. *Magn. Reson. Med.* **2017**, *77*, 2438−2443.

(4) Bobko, A. A.; Eubank, T. D.; Driesschaert, B.; Dhimitruka, I.; Evans, J.; Mohammad, R.; Tchekneva, E. E.; Dikov, M. M.; Khramtsov, V. V. Interstitial Inorganic Phosphate as a Tumor Microenvironment Marker for Tumor Progression. *Sci. Rep.* **2017**, *7*, No. 41233.

(5) Shevelev, G. Y.; Krumkacheva, O. A.; Lomzov, A. A.; Kuzhelev, A. A.; Rogozhnikova, O. Y.; Trukhin, D. V.; Troitskaya, T. I.; Tormyshev, V. M.; Fedin, M. V.; Pyshnyi, D. V.; Bagryanskaya, E. G. Physiological-Temperature Distance Measurement in Nucleic Acid using Triarylmethyl-Based Spin Labels and Pulsed Dipolar EPR Spectroscopy. *J. Am. Chem. Soc.* **2014**, *136*, 9874−9877.

(6) Yang, Z.; Liu, Y.; Borbat, P.; Zweier, J. L.; Freed, J. H.; Hubbell, W. L. Pulsed ESR Dipolar Spectroscopy for Distance Measurements in Immobilized Spin Labeled Proteins in Liquid Solution. *J. Am. Chem. Soc.* **2012**, *134*, 9950−9952.

(7) Tormyshev, V. M.; Chubarov, A. S.; Krumkacheva, O. A.; Trukhin, D. V.; Rogozhnikova, O. Y.; Spitsina, A. S.; Kuzhelev, A. A.; Koval, V.

V.; Fedin, M. V.; Godovikova, T. S.; Bowman, M. K.; Bagryanskaya, E. G. A Methanethiosulfonate Derivative of OX063 Trityl: a Promising and Efficient Reagent for SDSL of Proteins. *Chem. – Eur. J.* **2020**, *26*, 2705–2712.
(8) Ardenkjær-Larsen, J. H.; Fridlund, B.; Gram, A.; Hansson, G.; Hansson, L.; Lerche, M. H.; Servin, R.; Thaning, M.; Golman, K. Increase in signal-to-noise ratio of >10,000 times in liquid-state NMR. *Proc. Natl. Acad. Sci. U.S.A.* **2003**, *100*, 10158–10163.
(9) Niedbalski, P.; Kiswandhi, A.; Parish, C.; Wang, Q.; Khashami, F.; Lumata, L. NMR Spectroscopy Unchained: Attaining the Highest Signal Enhancements in Dissolution Dynamic Nuclear Polarization. *J. Phys. Chem. Lett.* **2018**, *9*, 5481–5489.
(10) Matsumoto, S.; Yasui, H.; Batra, S.; Kinoshita, Y.; Bernardo, M.; Munasinghe, J. P.; Utsumi, H.; Choudhuri, R.; Devasahayam, N.; Subramanian, S.; Mitchell, J. B.; Krishna, M. C. Simultaneous imaging of tumor oxygenation and microvascular permeability using Overhauser enhanced MRI. *Proc. Natl. Acad. Sci. U.S.A.* **2009**, *106*, 17898–17903.
(11) Kishimoto, S.; Krishna, M. C.; Khramtsov, V. V.; Utsumi, H.; Lurie, D. J. In Vivo Application of Proton-Electron Double-Resonance Imaging. *Antioxid. Redox Signal.* **2018**, *28*, 1345–1364.
(12) Poncelet, M.; Driesschaert, B. A ^{13}C-labeled triarylmethyl radical as EPR spin probe highly sensitive to molecular tumbling. *Angew. Chem., Int. Ed.* **2020**, DOI: 10.1002/anie.202006591.
(13) Hintz, H.; Vanas, A.; Klose, D.; Jeschke, G.; Godt, A. Trityl Radicals with a Combination of the Orthogonal Functional Groups Ethyne and Carboxyl: Synthesis without a Statistical Step and EPR Characterization. *J. Org. Chem.* **2019**, *84*, 3304–3320.
(14) Tan, X.; Ji, K.; Wang, X.; Yao, R.; Han, G.; Villamena, F. A.; Zweier, J. L.; Song, Y.; Rockenbauer, A.; Liu, Y. Discriminative Detection of Biothiols by Electron Paramagnetic Resonance Spectroscopy using a Methanethiosulfonate Trityl Probe. *Angew. Chem., Int. Ed.* **2020**, *59*, 928–934.
(15) Fleck, N.; Hett, T.; Brode, J.; Meyer, A.; Richert, S.; Schiemann, O. C–C Cross-Coupling Reactions of Trityl Radicals: Spin Density Delocalization, Exchange Coupling, and a Spin Label. *J. Org. Chem.* **2019**, *84*, 3293–3303.
(16) Jassoy, J. J.; Heubach, C. A.; Hett, T.; Bernhard, F.; Haege, F. R.; Hagelueken, G.; Schiemann, O. Site Selective and Efficient Spin Labeling of Proteins with a Maleimide-Functionalized Trityl Radical for Pulsed Dipolar EPR Spectroscopy. *Molecules* **2019**, *24*, No. 2735.
(17) Decroos, C.; Prangé, T.; Mansuy, D.; Boucher, J.-L.; Li, Y. Unprecedented ipso aromatic nucleophilic substitution upon oxidative decarboxylation of tris(p-carboxyltetrathiaaryl)methyl (TAM) radicals: a new access to diversely substituted TAM radicals. *Chem. Commun.* **2011**, *47*, 4805–4807.
(18) Driesschaert, B.; Levêque, P.; Gallez, B.; Marchand-Brynaert, J. Tetrathiatriarylmethyl Radicals Conjugated to an RGD-Peptidomimetic. *Eur. J. Org. Chem.* **2014**, *2014*, 8077–8084.
(19) Rogozhnikova, O. Y.; Vasiliev, V. G.; Troitskaya, T. I.; Trukhin, D. V.; Mikhalina, T. V.; Halpern, H. J.; Tormyshev, V. M. Generation of Trityl Radicals by Nucleophilic Quenching of Tris(2,3,5,6-tetrathiaaryl)methyl Cations and Practical and Convenient Large-Scale Synthesis of Persistent Tris(4-carboxy-2,3,5,6-tetrathiaaryl)-methyl Radical. *Eur. J. Org. Chem.* **2013**, *2013*, 3347–3355.
(20) Dhimitruka, I.; Velayutham, M.; Bobko, A. A.; Khramtsov, V. V.; Villamena, F. A.; Hadad, C. M.; Zweier, J. L. Large-scale synthesis of a persistent trityl radical for use in biomedical EPR applications and imaging. *Bioorg. Med. Chem. Lett.* **2007**, *17*, 6801–6805.
(21) Dhimitruka, I.; Grigorieva, O.; Zweier, J. L.; Khramtsov, V. V. Synthesis, structure, and EPR characterization of deuterated derivatives of Finland trityl radical. *Bioorg. Med. Chem. Lett.* **2010**, *20*, 3946–3949.
(22) Poncelet, M.; Huffman, J. L.; Khramtsov, V. V.; Dhimitruka, I.; Driesschaert, B. Synthesis of hydroxyethyl tetrathiatriarylmethyl radicals OX063 and OX071. *RSC Adv.* **2019**, *9*, 35073–35076.
(23) Song, Y.; Liu, Y.; Liu, W.; Villamena, F. A.; Zweier, J. L. Characterization of the binding of the Finland trityl radical with bovine serum albumin. *RSC Adv.* **2014**, *4*, 47649–47656.
(24) Bobko, A. A.; Dhimitruka, I.; Zweier, J. L.; Khramtsov, V. V. Trityl Radicals as Persistent Dual Function pH and Oxygen Probes for in Vivo Electron Paramagnetic Resonance Spectroscopy and Imaging: Concept and Experiment. *J. Am. Chem. Soc.* **2007**, *129*, 7240–7241.
(25) Taniguchi, H.; Madden, K. P. An in Situ Radiolysis Time-Resolved ESR Study of the Kinetics of Spin Trapping by 5,5-Dimethyl-1-pyrroline-N-oxide. *J. Am. Chem. Soc.* **1999**, *121*, 11875–11879.
(26) Neese, F. Software update: the ORCA program system, version 4.0. *WIRES Comput. Mol. Sci.* **2018**, *8*, No. e1327.
(27) Bowman, M. K.; Mailer, C.; Halpern, H. J. The solution conformation of triarylmethyl radicals. *J. Magn. Reson.* **2005**, *172*, 254–267.
(28) Driesschaert, B.; Robiette, R.; Lucaccioni, F.; Gallez, B.; Marchand-Brynaert, J. Chiral properties of tetrathiatriarylmethyl spin probes. *Chem. Commun.* **2011**, *47*, 4793–4795.
(29) Bobko, A. A.; Kirilyuk, I. A.; Grigor'ev, I. A.; Zweier, J. L.; Khramtsov, V. V. Reversible reduction of nitroxides to hydroxylamines: Roles for ascorbate and glutathione. *Free Radic. Biol. Med.* **2007**, *42*, 404–412.
(30) Tseytlin, O.; Guggilapu, P.; Bobko, A. A.; AlAhmad, H.; Xu, X.; Epel, B.; O'Connell, R.; Hoblitzell, E. H.; Eubank, T. D.; Khramtsov, V. V.; Driesschaert, B.; Kazkaz, E.; Tseytlin, M. Modular imaging system: Rapid scan EPR at 800 MHz. *J. Magn. Reson.* **2019**, *305*, 94–103.
(31) Driesschaert, B.; Bobko, A. A.; Khramtsov, V. V.; Zweier, J. L. Nitro-Triarylmethyl Radical as Dual Oxygen and Superoxide Probe. *Cell Biochem. Biophys.* **2017**, *75*, 241–246.
(32) Ranguelova, K.; Rice, A. B.; Khajo, A.; Triquigneaux, M.; Garantziotis, S.; Magliozzo, R. S.; Mason, R. P. Formation of reactive sulfite-derived free radicals by the activation of human neutrophils: An ESR study. *Free Radic. Biol. Med.* **2012**, *52*, 1264–1271.
(33) Ranguelova, K.; Chatterjee, S.; Ehrenshaft, M.; Ramirez, D. C.; Summers, F. A.; Kadiiska, M. B.; Mason, R. P. Protein Radical Formation Resulting from Eosinophil Peroxidase-catalyzed Oxidation of Sulfite. *J. Biol. Chem.* **2010**, *285*, 24195–24205.
(34) Mesa, J. A.; Velázquez-Palenzuela, A.; Brillas, E.; Torres, J. L.; Juliá, L. Synthesis of a new stable and water-soluble tris(4-hydroxysulfonyltetrachlorophenyl)methyl radical with selective oxidative capacity. *Tetrahedron* **2011**, *67*, 3119–3123.
(35) Joseph, B.; Tormyshev, V. M.; Rogozhnikova, O. Y.; Akhmetzyanov, D.; Bagryanskaya, E. G.; Prisner, T. F. Selective High-Resolution Detection of Membrane Protein–Ligand Interaction in Native Membranes Using Trityl–Nitroxide PELDOR. *Angew. Chem., Int. Ed.* **2016**, *55*, 11538–11542.
(36) Tan, K. O.; Mardini, M.; Yang, C.; Ardenkjær-Larsen, J. H.; Griffin, R. G. Three-spin solid effect and the spin diffusion barrier in amorphous solids. *Sci. Adv.* **2019**, *5*, No. eaax2743.
(37) Ahmad, R.; Kuppusamy, P. Theory, Instrumentation, and Applications of Electron Paramagnetic Resonance Oximetry. *Chem. Rev.* **2010**, *110*, 3212–3236.
(38) Komarov, D. A.; Dhimitruka, I.; Kirilyuk, I. A.; Trofimiov, D. G.; Grigor'ev, I. A.; Zweier, J. L.; Khramtsov, V. V. Electron paramagnetic resonance monitoring of ischemia-induced myocardial oxygen depletion and acidosis in isolated rat hearts using soluble paramagnetic probes. *Magn. Reson. Med.* **2012**, *68*, 649–655.
(39) Trukhin, D. V.; Rogozhnikova, O. Y.; Troitskaya, T. I.; Vasiliev, V. G.; Bowman, M. K.; Tormyshev, V. M. Facile and High-Yielding Synthesis of TAM Biradicals and Monofunctional TAM Radicals. *Synlett* **2016**, *27*, 893–899.
(40) Tormyshev, V. M.; Rogozhnikova, O. Y.; Bowman, M. K.; Trukhin, D. V.; Troitskaya, T. I.; Vasiliev, V. G.; Shundrin, L. A.; Halpern, H. J. Preparation of Diversely Substituted Triarylmethyl Radicals by the Quenching of Tris(2,3,5,6-tetrathiaaryl)methyl Cations with C-, N-, P-, and S-Nucleophiles. *Eur. J. Org. Chem.* **2014**, *2014*, 371–380.
(41) Decroos, C.; Li, Y.; Soltani, A.; Frapart, Y.; Mansuy, D.; Boucher, J.-L. Oxidative decarboxylation of tris-(p-carboxyltetrathiaaryl)methyl radical EPR probes by peroxidases and related hemeproteins: Intermediate formation and characterization of the corresponding cations. *Arch. Biochem. Biophys.* **2010**, *502*, 74–80.
(42) Driesschaert, B.; Robiette, R.; Le Duff, C. S.; Collard, L.; Robeyns, K.; Gallez, B.; Marchand-Brynaert, J. Configurationally Stable Tris(tetrathioaryl)methyl Molecular Propellers. *Eur. J. Org. Chem.* **2012**, *2012*, 6517–6525.